Error-Corrected Large-Signal Waveform Measurement System Combining Network Analyzer and Sampling Oscilloscope Capabilities

GÜNTER KOMPA, MEMBER, IEEE, AND FRIEDBERT VAN RAAY

Abstract — **A large-signal automatic stepped CW waveform measurement system for nonlinear device characterization is presented which combines the high accuracy of a vector network analyzer with the waveform measurement capabilities of a sampling oscilloscope. A large-signal error model and a corresponding coaxial calibration procedure are proposed to describe the systematic errors of the measurement setup. The error parameters and the correction algorithm are independent of the properties of the RF generator. System accuracy is investigated by Schottky diode verification measurements with different offsets toward the reference plane. GaAs MESFET reflection and transmission response measurements with error correction extended to the planar DUT reference planes are given.**

I. INTRODUCTION

THE ANALYSIS and design of nonlinear microwave circuits such as oscillators, power amplifiers, and frequency multipliers are based upon large-signal device models which may be derived from small-signal data under the quasi-static assumption. Until now there has been a lack of microwave measurement techniques which would yield a direct large-signal device characterization, providing amplitude and phase information of both the fundamental and the higher harmonics with respect to the device reference planes. Error-corrected large-signal waveform measurements are useful for nonlinear MESFET and MODFET model verification and may initiate new approaches in the direct access to the device large-signal behavior.

The large-signal microwave measurement methods so far reported in the literature (e.g. [1]–[5]) do not give any waveform information under large-signal periodic excitation conditions, with the exception of the CW measurement approaches recently proposed by Lott [6] and Sipilä *et al.* [7]. Lott describes a setup that comprises an HP 8410 network analyzer configuration for transmission measurements and an RF generator with internal multiplier for phase locking the network analyzer on the second, third, and fourth signal harmonic. Response-calibrated transmission measurement results of a packaged MESFET at a fundamental frequency of 5 GHz are presented without explicit consideration of source and load mismatches. For establishing the harmonic phase response calibration, a GaAs Schottky diode device is used as a nonlinear standard. Sipilä [7] uses a sampling oscilloscope for waveform observation of signals reflected and transmitted from the DUT under harmonic large-signal excitation. The error correction capabilities of this system are described, and measurement results concerning a silicon bipolar RF transistor at a frequency of 920 MHz are given.

In Sipilä's approach, the stimulus wave traveling toward the DUT is obtained from the measurement of a known short standard and the generator reflection coefficient, which has to be measured with a separate network analyzer. For reflection measurements, the phase difference between incident and reflected fundamental waves has to be evaluated from a one-channel oscilloscope waveform measurement. According to the experimental investigations of the authors using the same sampling oscilloscope as mentioned by Sipilä, the trigger drift will significantly influence this measurement at higher fundamental frequencies, e.g. 5 GHz and above.

The measurement system proposed in this paper uses a modified network analyzer one-path test unit for reference and test signal separation, yielding a simultaneous observation of stimulus and reflected waveforms. The concept of the system is to take the phase and magnitude relationship of the fundamental waves using the high accuracy of a vector network analyzer (VNA), while the signal amplitudes and waveforms are determined using a two-channel sampling oscilloscope. The calibration of the measurement system is directly supported by the vector network analyzer using a special one-path error model which takes into account the frequency-dependent behavior of the directional couplers and the tracking errors of the receiver systems. The error correction algorithm evaluates the stimulus, reflected, and transmitted waveforms at the DUT reference planes including source and load mismatch, tracking, and directivity errors.

In this paper, an automatic stepped CW measurement system suited for a fundamental excitation frequency range

Manuscript received July 11, 1989; revised November 20, 1989.
The authors are with the High-Frequency Engineering Department, University of Kassel, 3500 Kassel, West Germany.
IEEE Log Number 8933712.

0018-9480/90/0400-0358$01.00

from 1 GHz to about 7.5 GHz with 20 GHz maximum calibration frequency and up to 8 dBm (7 mW) RF power at the DUT is demonstrated. Using an additional power amplifier and appropriate hardware components, the input level could be increased up to the test set damage limit of about 1 W. Measurement accuracy is illustrated by a comparison of two one-port measurements of a Schottky diode using different offsets between the device and the reference plane of the calibrated system. In addition, some typical GaAs MESFET reflection and transmission measurements are shown with the error correction extended to the microstrip reference planes.

II. The Measurement Setup

The block diagram of the measurement setup under consideration is given in Fig. 1. A broad-band RF sweeper operating in stepped CW mode feeds a one-path large-signal test unit. The generator output reflection coefficient with a magnitude of about -10 dB [8] is diminished to about -20 dB by means of a 6 dB precision attenuator. The construction of the test unit is similar to that of a conventional network analyzer reflection/transmission test set, but provides the entire RF input power being transmitted to the "unknown" test port. The reflection or transmission measurement mode is selected by coaxial switches within the test unit. The test and reference channel outputs of the test unit monitor the incident wave traveling from the generator to the DUT, and the wave which is reflected or transmitted from the DUT via directional couplers. These outputs are connected to the NA frequency converter and the sampling heads of a dual-channel sampling oscilloscope via coax switches establishing good isolation between both of the receiver systems. The harmonic content of the test channel waveform does not influence the network analyzer fundamental frequency measurement because the down-conversion products of the harmonics do not fall into the relatively narrow band-pass region of the HP 8410 network analyzer IF amplifiers [9]. The directional couplers in the test unit, the external 20 dB precision attenuator in the transmission return path, and the additional 10 dB attenuators in front of the frequency converter inputs ensure that both receivers are in their linear operation region. These system features minimize the influence on the DUT when the positions of the receiver coax switches are changed.

Multiple-frequency measurements are supported by a count-down trigger circuit which enables the oscilloscope to trigger each measurement frequency automatically. This circuit comprises an injection-locked pulse oscillator whose fundamental frequency is tunable from 220 to 280 MHz. This tuning range ensures that every frequency above 1 GHz can be down-converted into a phase-synchronized subharmonic in this frequency range. With the count-down oscillator tuned to a fixed frequency, all harmonics of this frequency can be automatically triggered. The subharmonic synchronization is established by electronically fine-tuning the RF source and the count-down oscillator until both frequencies have nearly an integer ratio. This

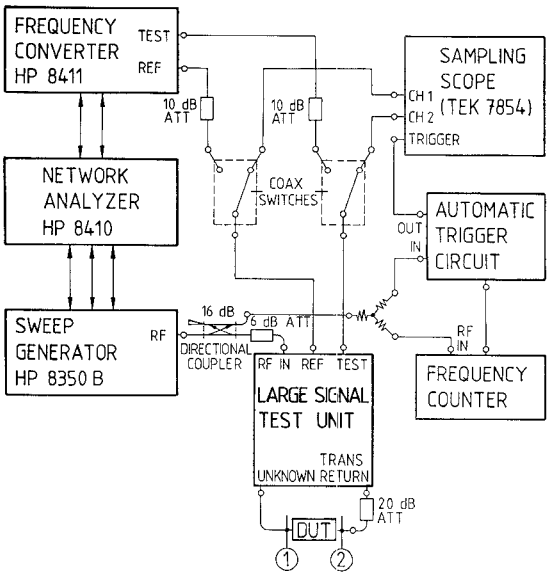

Fig. 1. Measurement setup.

can easily be achieved by the system controller in automatic measurements.

Prior to the measurements, the system is calibrated following the procedure described in Section IV. For establishing calibration data for all fundamental and harmonic measurement frequencies, the ratio between the minimum calibration frequency and the spacing between adjacent calibration frequencies is chosen to be an integer.

In actual one-port or two-port measurements, the reference channel monitors the incident wave traveling toward the DUT, and the test channel observes the wave being reflected or transmitted by the DUT, respectively. At first, the network analyzer measures the complex ratio of the fundamental waves in stepped CW operation. Subsequently, the coax switches are switched and the sampling oscilloscope records both the waveforms and gives the reference channel amplitude information. Recording the reference channel waveform enables the system to capture harmonics in the incident signal which may be caused either by harmonic reflections between DUT and the imperfectly matched generator or by the generator itself. These harmonics are then taken into account in the error correction algorithm to estimate the correct amplitude and phase values of the signal harmonics present at the DUT. For purposes of subsequent error correction, the reference and test channel waveforms of each measurement point are converted into the frequency domain using an FFT algorithm.

III. Large-Signal Error Model

The reflection test set shown in Fig. 2(a) is described as a linear four-port device characterized by the scattering matrix (S) with the RF input port 1, test port 2, and two receiver channel terminals 3 and 4, each corresponding to the physical connector reference plane. The receivers are assumed to be in their linear operation region, being described by the reflection coefficients ρ_3 and ρ_4. The

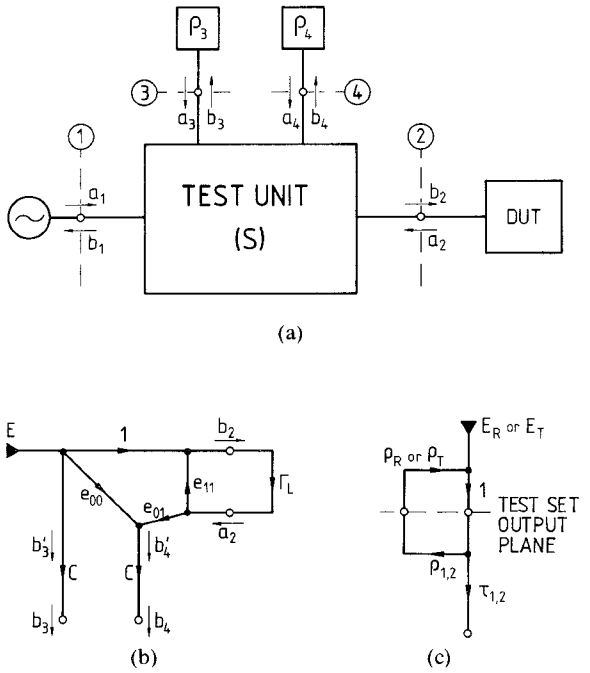

Fig. 2. Reflection test set description. (a) Four port description. (b) Equivalent flow graph diagram. (c) Receiver switching.

waves b_3 and b_4 are the measured waves b_{3_m} and b_{4_m} divided by the transmission factors of the receivers.

Next, the relation between the waves b_3, b_4 (b_{3_m}, b_{4_m} respectively) and the waves b_2, a_2 at the DUT reference plane for each spectral signal component is derived. For each signal frequency, the system can be described by the scattering matrix as follows:

$$\begin{pmatrix} b_1 \\ b_2 \\ b_3 \\ b_4 \end{pmatrix} = (S) \begin{pmatrix} a_1 \\ a_2 \\ \rho_3 b_3 \\ \rho_4 b_4 \end{pmatrix}. \tag{1}$$

Eliminating the variables a_1 and b_1 results in

$$\begin{aligned} S_{31}b_2 - S_{21}b_3 &= (S_{22}S_{31} - S_{21}S_{32})a_2 + (S_{23}S_{31} - S_{33}S_{21})\rho_3 b_3 \\ &\quad + (S_{24}S_{31} - S_{34}S_{21})\rho_4 b_4 \\ S_{41}b_2 - S_{21}b_4 &= (S_{42}S_{41} - S_{21}S_{42})a_2 + (S_{23}S_{41} - S_{43}S_{21})\rho_3 b_3 \\ &\quad + (S_{24}S_{41} - S_{14}S_{21})\rho_4 b_4. \end{aligned} \tag{2}$$

These simultaneous equations are rearranged for the variables b_2, a_2 and b_3, b_4, introducing formal coefficients $C_k (k = 1,6)$ for abbreviation, which depend on the scattering coefficients S_{ij} and the reflection coefficients ρ_3 or ρ_4:

$$\begin{aligned} S_{31}b_2 + C_1 a_2 &= C_2 b_3 + C_3 b_4 \\ S_{41}b_2 + C_4 a_2 &= C_5 b_3 + C_6 b_4. \end{aligned} \tag{3}$$

Solving (3) for the waves b_3 and b_4 results in a linear superposition of the waves b_2 and a_2 according to

$$\begin{aligned} b_3 &= Cb_2 + Da_2 \\ b_4 &= Ab_2 + Ba_2. \end{aligned} \tag{4}$$

The defined quantities A through D are constant complex coefficients which depend only on the test set S parameters and the receiver reflection coefficients. Equation (4) determines the relation between the measured waves b_3 and b_4 and the waves b_2 and a_2 at the DUT. For the derivation of the corresponding error model, it is assumed, in accordance with the notion that wave separation is inherent in a physical test set, that terminal 3 (Fig. 2(a)) is the reference channel output and terminal 4 is the test channel output of the test set. In this case, the wave quantity b_3 is essentially proportional to the input wave b_2 at the DUT, and b_4 is mainly determined by the reflected wave a_2. For a given physical nonideal test set, this means that parameters A through D are nonzero and that the relationships $|C| \gg |D|$ and $|B| \gg |A|$ are fulfilled.

Introducing wave quantities b_3' and b_4' with $b_{3,4} = C \cdot b_{3,4}'$ results in

$$\begin{aligned} b_3' &= b_2 + D/Ca_2 \\ b_4' &= A/Cb_2 + B/Ca_2. \end{aligned} \tag{5}$$

Equation (5) describes a bilinear transform between the wave ratios a_2/b_2 and b_4'/b_3' or the corresponding reflection coefficients, respectively. For this reason, (5) is equivalent to the well-known one-port error model for small-signal reflection measurement (e.g. [10]–[12]) using the error parameters e_{00}, e_{01}, and e_{11}. As shown above, an additional complex error parameter, the coupling factor C describing mainly the coupling attenuation of the directional couplers in the test set, must be introduced into the error model to maintain a correct description of the absolute values b_3, b_4 and b_2, a_2. This is illustrated in Fig. 2(b) by the large-signal error model flow graph. The signal E is only a virtual system stimulus and is not related to the physical properties of the RF source used in the real test system. In spite of that, the absolute values of each spectral component of b_2 and a_2 can be calculated if C, e_{00}, e_{01}, and e_{11} are known and the receivers are able to measure the absolute magnitudes and phase differences of each spectral component of the waves b_3 and b_4. Therefore, no information is required about the RF source.

The error model has to take into account the switching between the frequency converter and the sampling scope for both receiver channels. Regarding special stimulus and device conditions, the test set outputs can be described by two wave sources being approximately independent from each other due to the coupling factors and directivities of the directional couplers used in the test set. On the assumption that the source reflection coefficients ρ_R and ρ_T are not influenced by variations in the DUT or stimulus behavior, each of the test set outputs can be modeled by the equivalent flow graph given in Fig. 2(c) with $\rho_{1,2}$ and $\tau_{1,2}$ being the reflection and transmission coefficients of the receivers, with the indices describing the switch position. This switching model is equivalent to a single tracking error $T_{1,2}$ for each receiver given simply by

$$T_{1,2} = \frac{\tau_{1,2}}{1 - \rho_{R,T}\rho_{1,2}} \approx \tau_{1,2} \cdot (1 + \rho_{R,T} \cdot \rho_{1,2}). \tag{6}$$

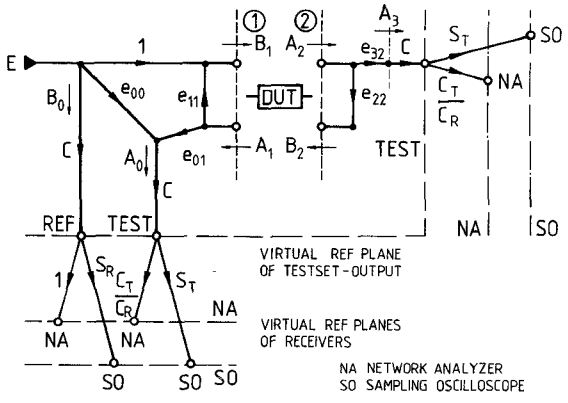

Fig. 3. Large-signal error model.

If the above-mentioned assumption is abandoned, the residual error can be estimated to be of the same order as the well-known receiver switching influence that is inherent in a one-path test set using a two-channel receiver. This error is discussed in [13] for various types of test sets.

For transmission measurements, the transmission return path of the test set is modeled by the error parameters e_{22} and e_{32}. The coupler tracking factor C was added in the return path to illustrate the power level difference between the DUT and receiver signal path. The large-signal error model flow graph used to describe the measurement system is presented in Fig. 3. S_T and S_R are the tracking errors of the two channels of the sampling oscilloscope system, and C_T/C_R is the network analyzer tracking error. The network analyzer is unable to take absolute amplitude measurements, so both channel tracking errors are collected in the factor C_T/C_R with the reference channel error set to a value of 1.

IV. Calibration

The steps of the calibration procedure are illustrated in Fig. 4. The system is calibrated using coaxial standards and a sinusoidal stimulus. In step 1, a usual one-path two-port calibration procedure [9], [11], [12], using sliding load, fixed load, open, short, and thru connection standards is performed. In step 2, the short calibration standard measurement is repeated with the channels of the network analyzer interchanged at the test set's reference and test channel outputs. Referring to the error model given in Fig. 3, the analyzer tracking error can be calculated from the values M_1 (short standard measurement, step 1) and M_2 (step 2) as follows:

$$(C_T/C_R)^2 = M_1 \cdot M_2 \rightarrow C_T/C_R = \pm\sqrt{M_1 M_2}. \qquad (7)$$

The determination of the sign of the complex square root requires an additional measurement of the network analyzer phase offset: The network analyzer is driven through a power divider connected to both channels via cables with balanced electrical lengths so that an approximated value for the phase offset can be determined. This approximated value permits the sign decision in (7) for each calibration frequency. In the next step, the absolute values of the sampling scope tracking errors for test and

STEP #	DESCRIPTION	MEASUREMENT CONFIGURATION	PARAMETER EXTRACTION
1	ONE - PATH TWO - PORT CALIBRATION	STANDARDS SHORT SLIDING LOAD OPEN THRU FIXED LOAD	e_{00}, e_{01}, e_{11} e_{22}, e_{32}
2	NA CHANNELS EXCHANGED	NA TEST REF. TEST REF. INPUT TEST UNIT UNKNOWN RETURN SHORT	C_T/C_R
3	• POWER METER AT REFERENCE CHANNEL • SAMPLING CHANNELS CONNECTED	SCOPE S_T S_R POWER METER TEST REF. INPUT TEST UNIT UNKNOWN SHORT	$\|S_R\|$, $\|S_T\|$
4	COUPLER TRACKING	NA TEST REF. TEST REF. INPUT UNKNOWN	C

Fig. 4. System calibration.

reference channel, $|S_T|$ and $|S_R|$, are determined. The difficulties in measuring the corresponding phase tracking errors were mentioned in [7]. Physical models or equivalent circuits exist only for special types of sampling diode configurations and a generalized measurement is not yet available [7], [14]. Therefore, the determination of the sampler phase tracking errors is omitted in our approach. With the short standard connected to the test port of the test set, the absolute power at the reference channel output is recorded with a power meter and converted into the voltage amplitude U_M at a 50 Ω load. Then the power meter is removed and both sampling oscilloscope channels are connected. The fundamental frequency amplitudes U_T and U_R are recorded using a Fourier transform of the displayed signals. The absolute value of S_R simply yields U_R/U_M. Taking into account the fact that the wave ratio of the waves in the physical test set output reference planes is independent of the receiver in use, $|S_T|$ turns out to be

$$|S_T| = \frac{U_T}{U_R} \cdot \frac{|C_T/C_R|}{|M_1|} \cdot |S_R|. \qquad (8)$$

Step 4 evaluates the coupler tracking factor C. A precision attenuator is inserted between the source and the test unit. The network analyzer channels are connected to the "unknown" test port and the reference output of the test unit using two identical cables to ensure nearly the same cable attenuation on both channels. In this way the measurement gives a good approximation of the absolute value of coupler tracking C. Referring to the error model, $|C|$ turns

out to be

$$|C| = |C_T/C_R|/|M_{4_a}| \tag{9}$$

with M_{4_a} being the corresponding network analyzer measurement value.

The argument of C cannot be measured directly because the hardware configuration requires a cable in front of at least one network analyzer channel. Assuming that the cable length difference between the two channels is not dispersive, a frequency-linear phase shift is added to the argument of C. This will not influence the waveforms in the test system, so that it can be ignored for our purposes. With this cable length suitably chosen, the coupler phase dispersion is measured and the argument of the coupler tracking error C is calculated from the measurement value M_{4_b} by

$$\arg(C) = -\arg(M_{4_b}) + \arg(C_T/C_R). \tag{10}$$

Finally, the parameters e_{00}, e_{01}, e_{11} and e_{22}, e_{32} of the error model are determined from the one-path two-port calibration procedure performed in step 1. To obtain these parameters in accordance with the above-mentioned error model, each measurement value is divided by the analyzer tracking error C_T/C_R.

It should be noticed that only the determination of the coupler tracking C requires the network analyzer tracking error C_T/C_R to be explicitly known. For error-corrected measurement purposes, it is sufficient to know the sampling scope tracking errors relative to the network analyzer tracking error and the other error parameters. All error parameters with the exception of C are exactly evaluated in accordance with the error model derived in Section III.

The error correction algorithm used in the approach discussed is different from that proposed by Sipilä *et al.* [7]. The goal is to calculate the waveform spectra in the DUT coaxial reference planes. Let $A_m(k)$ and $B_m(k)$ be the test and reference wave voltage Fourier coefficients of the kth harmonic in the receiver measurement planes. The following data are measured by the receivers:

$S = A_m(1)/B_m(1)$	Measured by the network analyzer.
$\|B_m(1)\|$ and $B_m(k), k>1$	FFT of reference signal recorded by the sampling scope with phase coefficients normalized to $\arg(B_m(1)) = 0$.
$A_m(k), k>1$	FFT of test signal with phase coefficients normalized to the network analyzer fundamental phase value.
$\|A_m(1)\|$	This coefficient of the test signal FFT is not utilized. Instead, the complex value $A_m(1)$ is computed from $\|B_m(1)\|$ and the network analyzer measurement value S using $A_m(1) = S\|B_m(1)\|$.

Referring to the error model and the phase coefficient

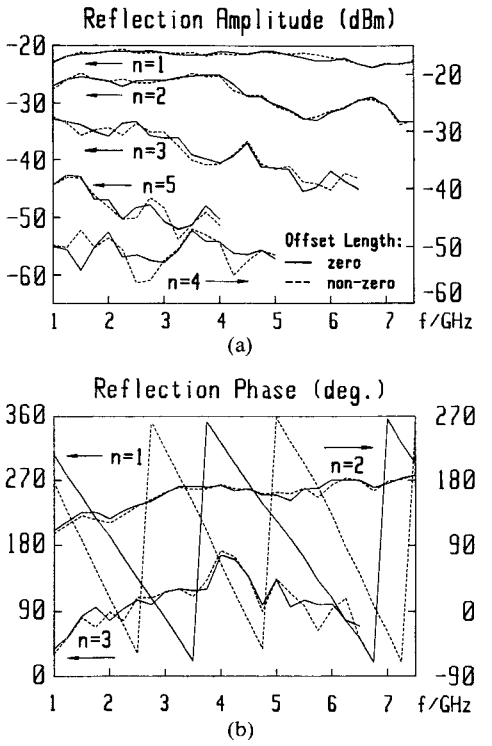

Fig. 5. Uncorrected Schottky diode verification measurements: (a) amplitude; (b) phase.

normalization, these measured signals can be composed in the test set output planes using the tracking factors S_R, S_T, and (C_T/C_R). Multiplication by the coupling factor C maintains the waves denoted A_0, B_0, and A_3 in Fig. 3. Subsequently, the waves are transformed to the waves A_1, B_1, A_2, and B_2 in the DUT reference planes for each harmonic as follows:

$$B_1 = \left(1 - \frac{e_{11}e_{00}}{e_{01}}\right)B_0 + \frac{e_{11}}{e_{01}}A_0$$

$$A_1 = -\frac{e_{00}}{e_{01}}B_0 + \frac{1}{e_{01}}A_0$$

$$A_2 = A_3/e_{32} \qquad B_2 = \frac{e_{22}}{e_{32}}A_2. \tag{11}$$

It should be mentioned that the correction algorithm does not require any information about the source stimulus used in the actual test setup, which may be nonlinear in its reflection coefficient and harmonic signal content. In this point, the restrictions mentioned in [7] have been overcome by our approach.

V. Verification Measurements

In this section, the performance of the system is demonstrated by a comparison of two one-port large-signal reflection measurements. Because of the lack of a nonlinear standard, a Schottky diode device was measured with a zero- and a nonzero-length thru connection between the DUT and the coaxial reference plane. The latter has been realized by a coax adapter in front of the DUT.

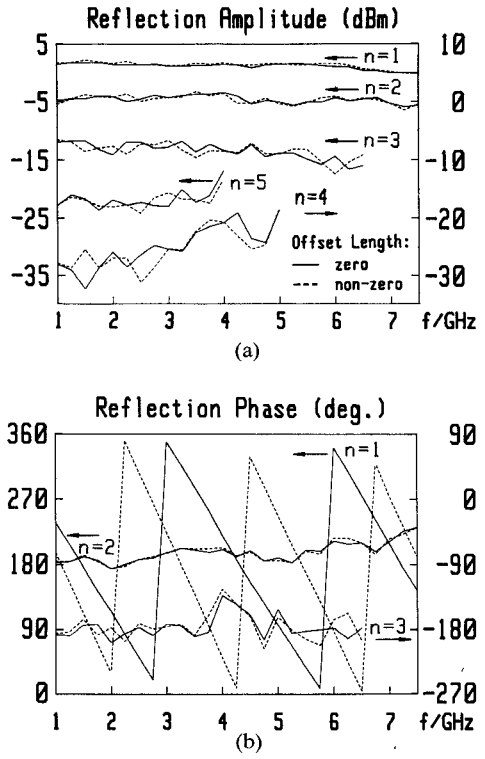

Fig. 6. Error-corrected Schottky diode verification measurements: (a) amplitude; (b) phase

The raw data results are shown in Fig. 5 and the error-corrected measurement results are given in Fig. 6, displaying amplitude and phase coefficients of the fundamental and higher harmonics in the fundamental frequency range from 1 GHz to 7.5 GHz. The upper frequency limits for the harmonics correspond to the maximum calibration frequency of 20 GHz. The phase coefficients of the higher harmonics are normalized to the fundamental phase coefficient for better visibility of the phase behavior of the nonlinear DUT. The strong frequency dependence of the wave amplitudes in the uncorrected curves is due to sampler and directional coupler tracking errors. These errors are eliminated by the correction, as well as the coupler phase dispersion, which can be found in the uncorrected phase traces of the second and third harmonics at lower fundamental frequencies up to around 2.5 GHz.

The curve ripple is primarily due to source mismatch and power variations versus frequency. The reflection interactions between the DUT and the test set and source configuration are influenced when the coax adapter is inserted in the signal path. For this reason, large-signal measurements of any nonlinear DUT with different electrical lengths between the device and the system reference plane give exactly the same results only if the equivalent source seen by the DUT provides a negligible reflection coefficient.

According to the error model, the parameters e_{ij} in connection with the tracking error C_T/C_R represent a conventional test set configuration yielding a fundamental wave ratio measurement accuracy that is equal to that of a typical small-signal network analyzer configuration with error correction included. Additional errors in the error-corrected determination of the fundamental wave amplitude and the amplitude and phase coefficients of the nonfundamental harmonics depend on the FFT systematic and random errors and on the total tracking error, consisting of the uncertainty in the parameters C and S_T or S_R respectively.

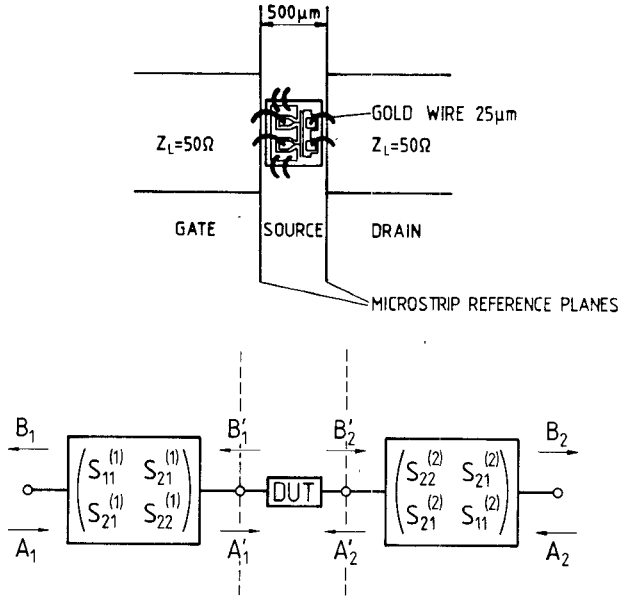

Fig. 7. Sketch of test fixture and microstrip reference planes.

VI. Large-Signal Transistor Measurements

The transmission and reflection behavior of a MESFET chip NE 71000 was measured with different input power levels at the DUT coaxial input reference plane. In this measurement, the chip was mounted in a test fixture which was previously characterized on a HP 8510 network analyzer using the microstrip THLR calibration technique published earlier by the authors [15], [16].

Fig. 7 displays the microstrip DUT reference plane definition and the equivalent representation of the test fixture. The wave quantities A_1', B_1', A_2', B_2' at the inner reference planes can be evaluated from the data A_1, B_1, A_2, B_2 with the S parameters of both fixture halves already known as follows:

$$\begin{pmatrix} B_\mu \\ A_\mu' \end{pmatrix} = (S^{(\mu)}) \cdot \begin{pmatrix} A_\mu \\ B_\mu' \end{pmatrix} \tag{12}$$

$$A_\mu' = \left(S_{21}^{(\mu)} - \frac{S_{11}^{(\mu)} S_{22}^{(\mu)}}{S_{21}^{(\mu)}} \right) \cdot A_\mu + \frac{S_{22}^{(\mu)}}{S_{21}^{(\mu)}} B_\mu \tag{13}$$

$$B_\mu' = -\frac{S_{11}^{(\mu)}}{S_{21}^{(\mu)}} \cdot A_\mu + \frac{1}{S_{21}^{(\mu)}} B_\mu \qquad \text{with } \mu = 1,2. \tag{14}$$

In addition to the microstrip calibration technique [15], the parameters $S_{21}(\mu)$ are obtained from $S_{21}^{(\mu)2}$ computing the delay between the coaxial and microstrip reference planes for sign decision.

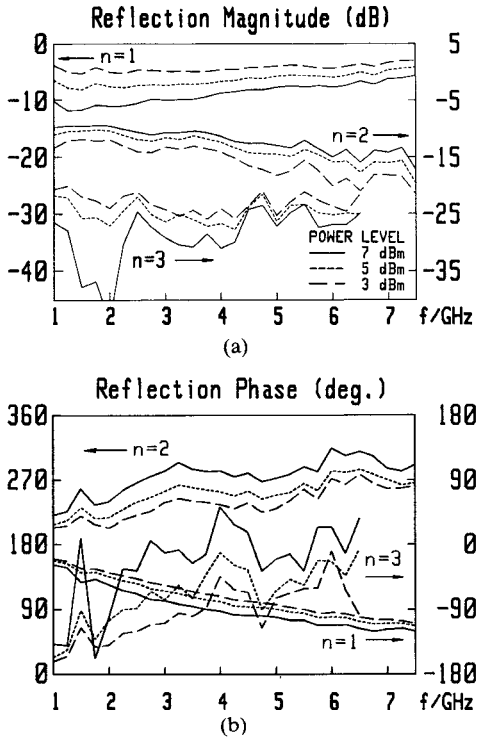

Fig. 8. GaAs MESFET reflection measurement: (a) magnitude; (b) phase.

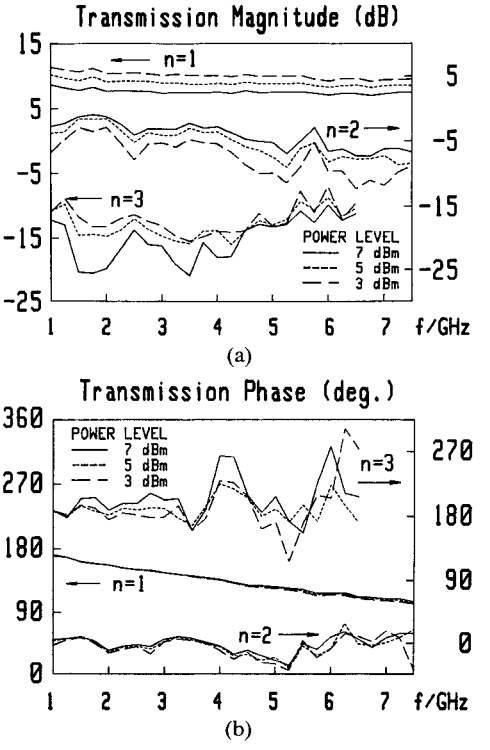

Fig. 9. GaAs MESFET transmission measurement: (a) magnitude; (b) phase.

Figs. 8 and 9 illustrate the frequency-dependent reflection and transmission behavior of the MESFET NE 71000 regarding the microstrip reference planes with the RF input power level as parameter. The bias conditions are $U_{GS} = 0.3$ V, $U_{DS} = 2$ V, and $I_{DS} = 63$ mA (with RF power switched off). The graphic representation is the same as mentioned for Figs. 5 and 6. The magnitude spectra scaling was chosen as the ratio between the wave amplitude and the fundamental frequency stimulus amplitude for better demonstration of the input power sensitivity of the nonlinear DUT. Considering the increasing input power levels, the magnitude diagrams make it evident that the energy of the response signal components is shifted from the first and third harmonic to the second harmonic for reflection and transmission measurement. In the reflection phase measurement, a strong sensitivity of the fundamental and higher harmonic phase coefficients versus increasing input power level is observed.

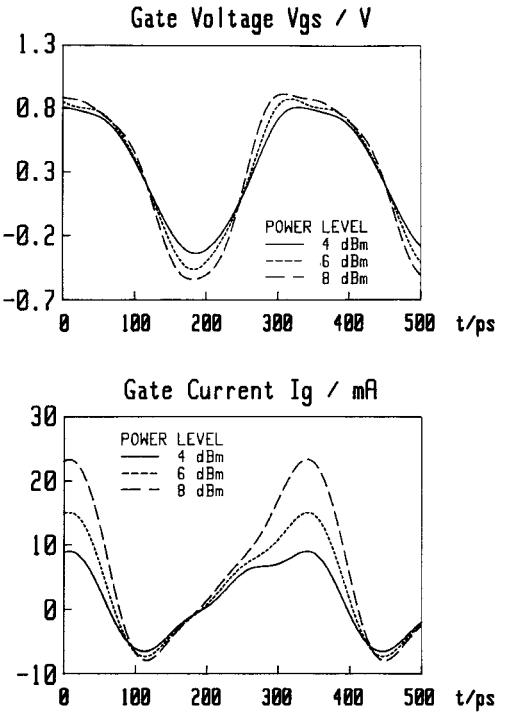

Fig. 10. GaAs MESFET gate voltage and current.

For further investigation and modeling purposes, the measurement results were transformed in the time domain at distinct frequencies. The voltage and current waveforms at the DUT input reference plane are presented in Fig. 10 for a fundamental frequency of 3 GHz and different input power levels. Based upon a simple nonlinear equivalent circuit of the gate–source region of the FET, the characteristics of the circuit elements were evaluated from the time-domain signal representation. The results for the most part agree with the gate-voltage-dependent resistive and capacitive nonlinearities obtained from small-signal measurements using the same equivalent circuit under the quasi-static assumption.

VII. Conclusions

A large-signal stepped CW waveform measurement system has been presented which combines the high accuracy of a vector network analyzer with the waveform measurement capabilities of a sampling oscilloscope system. The network analyzer supports the system calibration and fundamental wave ratio measurement, while the oscilloscope records the incident and response waveforms and gives the

amplitude information concerning the stimulus wave. A measurement setup suited for automatic reflection and transmission measurements in the fundamental frequency range from 1 to 7.5 GHz has been described.

A large-signal error model and a special calibration procedure have been developed. The error correction algorithm transforms the measurement data into the frequency-domain wave quantities at the coaxial reference planes of the DUT. System accuracy is demonstrated by a comparison of two Schottky diode measurements using different through lines between system and DUT reference planes.

The applicability of the measurement system is illustrated by a GaAs MESFET reflection and transmission measurement with error correction extended to the microstrip reference planes using the THLR microstrip deembedding technique published earlier.

The spectral representation of the error-corrected nonlinear system responses yields a direct access to the large-signal device behavior. The higher harmonic phase spectra generally contain information with respect to the separation of the device nonlinearities into resistive and reactive components. The time-domain waveform representation will be a useful instrument for large-signal modeling and model verification of nonlinear active devices.

REFERENCES

[1] W. H. Leighton, R. J. Chaffin, and J. G. Webb, "RF amplifier design with large signal *S*-parameters," *IEEE Trans. Microwave Theory Tech.*, vol. MTT-21, pp. 809–814, Dec. 1973.

[2] Sr. Mazumder and P. D. van der Puije, "'Two-signal' method of measuring the large signal S-parameters of transistors," *IEEE Trans. Microwave Theory Tech.*, vol. MTT-26, pp. 417–420, June 1978.

[3] R. S. Tucker and P. D. Bradley, "Computer-aided error correction of large-signal load-pull measurement," *IEEE Trans. Microwave Theory Tech.*, vol. MTT-32, pp. 296–300, Mar. 1984.

[4] I. Hecht, "Improved error-correction technique for large-signal load-pull measurements," *IEEE Trans. Microwave Theory Tech.*, vol. MTT-35, no. 11, pp. 1060–1062, Nov. 1987.

[5] W. Filensky, "Großsignal-Zeitbereichsverhalten von GaAs-MESFETs," Doctoral thesis, Technical University of Aachen, Institute of Semiconductor Electronics, Aachen, West Germany, 1979.

[6] U. Lott, "A method for measuring magnitude and phase of harmonics generated in nonlinear-microwave two-ports," in *IEEE MTT-S, Int. Microwave Symp. Dig.* (New York), 1988, pp. 225–228.

[7] M. Sipilä, K. Lethinen, and V. Porra, "High-frequency periodic time-domain waveform measurement system," *IEEE Trans. Microwave Theory Tech.*, vol. 36, pp. 1397–1405, Oct. 1988.

[8] *Hewlett Packard HP 83525A RF Plug-In Operating and Service Manual*, Hewlett Packard Company, Santa Rosa, CA, 1981.

[9] Hewlett Packard, "Vektorielle Messungen im HF-Bereich," seminar documents, 1987.

[10] O. Davies, R. B. Doshi, and B. Nagenthiram, "Correction of microwave network analyzer measurements of two-port devices," *Electron. Lett.*, vol. 9., no. 23, pp. 543–544, 1973.

[11] S. Rehnmark, "On the calibration process of automatic network analyzer systems," *IEEE Trans. Microwave Theory Tech.*, vol. MTT-22, pp. 457–458, Apr. 1974.

[12] R. A. Hackborn, "An automatic network analyzer system," *Microwave J.*, vol. 11, no. 5, pp. 45–52. May 1968.

[13] A. A. M. Saleh, "Explicit formulas for error-correction in microwave measuring sets with switching-dependent port mismatches," *IEEE Trans. Instrum. Meas.*, vol. IM-28, pp. 67–71, Mar. 1979.

[14] S. M. Riad, "Modeling of the HP 1430A feedthrough wideband (28-ps) sampling head," *IEEE Trans. Instrum. Meas.*, vol. 31, pp. 110–115, June 1982.

[15] G. Kompa and M. Schlechtweg, "Broadband and high-accurate GaAs FET characterization in microstrip medium up to 26.5 GHz," presented at 4th Conf. Microwave and Optoelectronics (MIOP), 28.3.-2.3.89, Sindelfingen, West Germany, paper 2A.6.

[16] G. Kompa, M. Schlechtweg, and F. van Raay, "Precisely calibrated coaxial-to-microstrip transitions yield improved performance in GaAs FET characterization," *IEEE Trans. Microwave Theory Tech.*, vol. 38, pp. 62–68, Jan. 1990.

Günter Kompa (M'89) received the M.S. (1970) and Ph.D. (1975) degrees, both in electrical engineering, from the University of Aachen (RWTH). In his thesis he treated microstrip discontinuity problems using the planar waveguide model.

In 1976 he joined the Measurement and Control Research Division of Endress and Hauser in Maulburg, West Germany, where he was engaged in short-range microwave and laser radar development. He developed the first eye-safe pulsed laser radar with millimeter accuracy for level control measurement using the relaxation oscillation of semiconductor diodes. In 1984, he became Professor of Electrical Engineering at the University of Kassel, where he is teaching and doing research in electromagnetic theory, microwave techniques, measurement techniques, and GaAs device modeling.

Dr. Kompa has published and presented more than 30 technical papers on MIC design, GaAs device characterization and modeling, and radar-type sensors. In 1978, he contributed a paper to the Special M.I.C. Issue of *The Radio and Electronic Engineer* entitled "Design of Stepped Microstrip Components," which gained him the Heinrich Hertz Premium. He has filed numerous patents in Europe, the U.S., and Japan, mainly on various radar-type sensors.

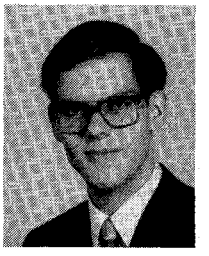

Friedbert van Raay was born in Hilden, West Germany, on December 16, 1960. He received the diploma (M.S. degree) in electrical engineering in 1984 from the Technical University of Aachen, West Germany.

In 1984, he worked on passive broad-band microstrip lumped-element structures at the Institute of Semiconductor Electronics, Technical University Aachen. In 1985 he joined the High Frequency Engineering Department of the University of Kassel, West Germany, where he is currently working on large-signal measurement techniques at microwave frequencies.